Published in final edited form as:
Biochemistry. 2012 January 31; 51(4): 879–887. doi:10.1021/bi201768v.

Essential Role of the Donor Acyl Carrier Protein in Stereoselective Chain Translocation to a Fully Reducing Module of the Nanchangmycin Polyketide Synthase†

Xun Guo[1], **Tiangang Liu**[2], **Zixin Deng**[2,3], and **David E. Cane**[1,*]

[1]Department of Chemistry, Box H, Brown University, Providence, Rhode Island 02912-9108, USA

[2]Key Laboratory of Combinatorial Biosynthesis and Drug Discovery (Wuhan University), Ministry of Education, and Wuhan University School of Pharmaceutical Sciences, Wuhan 430071, P. R. China

[3]Key Laboratory of Microbial Metabolism and School of Life Sciences & Biotechnology, Shanghai Jiaotong University, Shanghai 200030, P. R. China

Abstract

Incubation of recombinant module 2 of the polyether nanchangmycin synthase (NANS), carrying an appended thioesterase domain, with the ACP-bound substrate (2*RS*)-2-methyl-3-ketobutyryl-NANS_ACP1 (**2-ACP1**) and methylmalonyl-CoA in the presence of NADPH gave diastereomerically pure (2*S*,4*R*)-2,4-dimethyl-5-ketohexanoic acid (**4a**). These results contrast with the previously reported weak discrimination by NANS module 2+TE between the enantiomers of the corresponding *N*-acetylcysteamine-conjugated substrate analogue (±)-2-methyl-3-ketobutyryl-SNAC (**2-SNAC**), which resulted in formation of a 5:3 mixture of **4a** and its (2*S*,4*S*)-diastereomer **4b**. Incubation of NANS module 2+TE with **2-ACP1** in the absence of NADPH gave unreduced 3,5,6-trimethyl-4-hydroxypyrone (**3**) with a k_{cat} of 4.4±0.9 min^{-1} and a k_{cat}/K_m 67 min^{-1} mM^{-1}, corresponding to a ~2300-fold increase compared to the k_{cat}/K_m for the diffusive substrate **2-SNAC**. Covalent tethering of the 2-methyl-3-ketobutyryl thioester substrate to the NANS ACP1 domain derived from the natural upstream PKS module of the nanchangmycin synthase significantly enhanced both the stereospecificity and the kinetic efficiency of the sequential polyketide chain translocation and condensation reactions catalyzed by the ketosynthase domain of NANS module 2.

Modular polyketide synthases (PKSs) are multifunctional megaproteins that are responsible for the assembly line biosynthesis of an enormous variety of highly complex natural products (1, 2), including many important medicinals with antibiotic, anticancer, antiparasitic, or immunosuppressive activity as well as numerous agriculturally important agents. In a typical modular PKS, each module is responsible for a single round of polyketide chain elongation and functional group modification, with the number of modules directly corresponding to the number of incorporated ketide building blocks. Each

†This work was supported by National Institutes of Health Grant GM22172 to D.E.C., by the 973 Project from the Ministry of Science and Technology of China (2012CB721001) and the National Science Foundation of China (31170096 and 31040086) to T. L., and by grants 973 and 863 from the Ministry of Science and Technology of China to Z. D.

Address correspondence to D.E.C.: tel: +1-401-863-3588; david_cane@brown.edu.

CONFLICT OF INTEREST STATEMENT: None of the authors (X Guo, T Liu, Z Deng, DE Cane) have any conflict of interest.

SUPPORTING INFORMATION AVAILABLE

Polyether and macrolide structures, SDS-PAGE, ESI-MS, LC-MS, and GC-MS data, and kinetic plots. This material is available free of charge at http://pubs.acs.org.

homodimeric module contains a minimum of three core domains (Figure 1A): 1) an acyl carrier protein (ACP) with a phosphopantetheine prosthetic group that carries each of the covalently tethered polyketide biosynthetic intermediates from one catalytic domain to the next within each module and then delivers the mature polyketide chain extension product to the ketosynthase (KS) domain of the downstream module; 2) an acyltransferase (AT) domain that specifically catalyzes transthioesterification of the appropriate malonyl or methylmalonyl-CoA chain elongation substrate onto the terminal cysteamine thiol of the ACP phosphopantetheinyl arm; and 3) a β-ketoacyl-ACP synthase (ketosynthase or KS) domain that is responsible for the central polyketide chain-building reaction, consisting of initial translocation of the electrophilic polyketide acyl thioester substrate donated by the ACP domain of the upstream module, by transesterification to the active site cysteine residue of the ketosynthase, followed by KS-catalyzed decarboxylative condensation with the nucleophilic malonyl- or methylmalonyl chain extender that is attached to the ACP domain of the paired subunit of the homodimeric protein (Figure 1A). Varying combinations of optional ketoreductase (KR), dehydratase (DH), and enoylacyl-ACP reductase (ER) domains are responsible for the characteristic β-ketoacyl-modifying reactions of each chain-elongation cycle (2).

For many years, the ~100–150-amino acid (~12–18 kDa) ACP domains of polyketide and fatty acid synthases had been thought to be more or less inert carriers of the various reaction intermediates, with the flexible 20-Å phosphopantetheinate group serving to shuttle intermediates from the active site of one catalytic domain to another (3). A wealth of recent kinetic and protein structural findings have considerably altered this picture. For example, ACPbound electrophilic diketide substrates have k_{cat}/K_m values for KS-catalyzed chain elongation that are 3 orders of magnitude greater than those of the corresponding *N*-acetylcysteamine (SNAC) analogs, largely but not exclusively due to 1000-fold reductions in the K_m for the reaction (4, 5). The observed k_{cat}/K_m is itself dominated by the second order rate-constant for KS-catalyzed acylation of its active site cysteine by the electrophilic substrate (6). The crystal structures of two KS–AT didomains from the 6-deoxyerythonolide B synthase (DEBS) (7–9) as well as those of a mammalian fatty acid synthase (10–12) have all revealed that the active sites of the respective KS and AT domains are rigidly separated by >80 Å. A static ACP domain cannot therefore shuttle intermediates between the KS and AT active sites solely by pivoting only the 20-Å pantetheine side chain, thus requiring considerable additional segmental motion of the ACP domain itself. Most recently, extensive mutational dissection of ACP domains from the 6-deoxyerythronolide B synthase (DEBS) has established that specific loop regions of the ACP four-helix bundle are involved in highly specific protein-protein interactions with specific docking surfaces of the paired KS domains and that *distinct* regions of the ACP domain are responsible for the specificity of intermodular chain translocation compared to intramodular condensative chain elongation (13, 14). In addition, ACP domains have also been shown to play a critical role in the maintaining the observed stereospecificity of KR-catalyzed reductions while significantly augmenting both the chemical and configurational stability of the ACP-bound α-methyl-β-ketoacyl thioester substrates (15, 16). Finally, ACP-bound substrates have also been found to be strongly preferred over their SNAC analogues as substrates for recombinant DH domains (17, 18).

We recently described the first recombinant expression and biochemical characterization of a discrete, fully saturating PKS module (19). Nanchangmycin synthase (NANS) module 2, encoded by the *NanA2* gene of *Streptomyces nanchangensis* and harboring the full suite of β-carbon processing KR, DH, and ER domains, catalyzes the second round of polyketide chain elongation and reduction in the biosynthesis of the anticoccidial polyether nanchangmycin (**1**) (20, 21) (Figure 1). Incubation of the racemic *N*-acetylcysteamine substrate analogue (±)-2- methyl-3-ketobutyryl-SNAC (2-methylacetoacetyl-SNAC, **2-**

SNAC) and methylmalonyl-CoA with recombinant NANS module 2+TE carrying an appended DEBS thioesterase (TE) domain yielded 3,5,6-trimethyl-4-hydroxypyrone **3**, resulting from enol-lactonization of the initially formed 3,5-diketo-2,4-dimethylhexanoyl-ACP intermediate (19) (Figure 2A-a). Inclusion of NADPH in the incubation mixture gave, in addition to hydroxypyrone **3**, a 5:3 mixture of (2*S*,4*R*)-2,4-dimethylhexanoic acid (**4a**), the predicted triketide product of the full ketoreduction– dehydration–enoylreduction sequence, unexpectedly accompanied by the corresponding (2*S*,4*S*)- diastereomer **4b**. The identity and stereochemistry of both **4a** and **4b** were established by a combination of LC-MS and chiral GC-MS on the derived methyl esters **4a**-**Me** and **4b**-**Me**, including direct comparison with authentic synthetic standards of each methyl ester (Figure 2A–b). The NANS KS2 domain is thus apparently unable to discriminate cleanly between (2*S*)-**2-SNAC**, the diffusive SNAC analogue of its native (2*S*)-2-methyl-3-ketobutyryl-ACP1 substrate, and its unnatural enantiomer (2*R*)-**2-SNAC**. Notably, NANS ER2, which sets the exclusively observed (2*S*)-2-methyl configuration of the saturated triketide product (Figure 1), stereospecifically reduced the 2-methylenoyl double bond of both the natural and the unnatural 4-methyl epimers of the transiently generated (*E*)-2,4-dimethyl-5-ketohex-2-enoyl-ACP2 intermediate. In separate incubations with recombinant NANS DH2, we also established that this dehydratase catalyzes the stereospecific *syn* dehydration exclusively of (2*R*,*3R*)-2-methyl-3- hydroxyacyl-ACP substrates to the corresponding (*E*)-2-methyl-2-enoyl-ACP products, thereby revealing the previously cryptic stereochemistry of both the reduction product that normally is generated by the upstream NANS KR2 domain as well as the geometry of the dehydration product that must subsequently serve as the substrate for the downstream ER2 domain (19) (Figure 1).

The failure of recombinant NANS module 2+TE to distinguish between the enantiomers of the diffusive (*2RS*)-*2*-methyl-3-ketobutyryl-SNAC substrate analogue (**2-SNAC**) was unexpected, since the nanchangmycin synthase normally produces a single diastereomer of the natural polyether *in vivo*. In principle, NANS module 1 might only produce a single enantiomer of the 2- methyl-3-keto diketide substrate, and the observed *in vitro* lack of discrimination between the two enantiomers of **2-SNAC** by NANS module 2 might simply have reflected an intrinsic lack of stereoselectivity by the downstream NANS KS2 domain. On the other hand, it is far more likely that for NANS KS2 to exercise its intrinsic stereospecificity, it is necessary that the electrophilic substrate for chain translocation be tethered to an ACP domain, as it is during *in vivo* biosynthesis, so as to insure proper orientation and processing of the substrate. In order to distinguish between these possibilities and to better understand the molecular basis for the requisite chain elongation stereospecificity, we have now used a chemoenzymatically prepared sample of (±)-(*2RS*)-2-methyl-3-ketobutyryl-ACP1 (**2-ACP1**) to reveal the critical role of the ACP partner domain in KS-mediated recognition of the electrophilic substrate, resulting in the complete control of the stereospecificity of the NANS KS2-catalyzed polyketide chain translocation and chain elongation reactions.

EXPERIMENTAL PROCEDURES

Methods

All DNA manipulations were performed following standard procedures (22). DNA sequencing was carried out at the U. C. Davis Sequencing Facility, Davis, CA. All proteins were handled at 4 °C unless otherwise stated. Protein concentrations were determined according to the method of Bradford, using a Hewlett Packard 8452A Diode Array UV/Vis spectrophotometer with bovine serum albumin as the standard (23). Protein purity was estimated using SDS PAGE gel electrophoresis and visualized using Coomassie Blue stain according to the method of Laemmli (24). Phosphorimaging was carried out using Bio-Rad Kodak-series screens and a Bio- Rad FX-Pro Molecular Imager and data were analyzed

using the software Quantity One. ^{1}H NMR (400 MHz) and ^{13}C NMR (75 and 100 MHz) spectra were obtained with Bruker Avance AM 300 and AM 400 spectrometers. Chemical shifts are referenced to $CDCl_3$ at room temperature. High resolution LC-ESI-MS and ESI-MS-MS spectra were recorded on a Thermo LXQ LC-ESI-MS equipped with an Agilent Eclipse XDB-C18 column (2.1 mm×150 mm, 3.5 μm). Optical rotations were recorded using a Jasco P1010 polarimeter. Kinetic data were analyzed by direct fitting to the Michaelis-Menten equation using Kaleidagraph software. Reported standard deviations in the steady-state kinetic parameters represent the calculated statistical errors in the non-linear, least-squares regression analysis. High resolution FAB MS were determined on a JEOL JMS 600 (EI, positive ion mode). GC-MS analysis was performed on a GC-MS Hewlett-Packard Series 2 GC-MSD, He at 1mL/min, 70 eV EI in positive ion mode with a Varian CP-Chiralsil-DEX CB capillary column, 25 m × 0.32 mm. GC-MS and LC-MS assays of incubations of NANS module 2+TE with (2*RS*)-2-methyl-3-ketobutyryl-SNAC ((±)-**2**-SNAC) both with and without added NADPH were carried out as previously described (19).

Materials

Reagents purchased from Sigma-Aldrich were of the highest quality available and were used without further purification. [2-^{14}C]Methylmalonyl-CoA (50 mCi/mmol) was purchased from American Radiolabeled Chemicals. Amicon Ultra cellulose centrifugal filters were from Millipore. Aluminum-backed thin-layer chromatography plates (250 μm) were purchased from Whatman. SDS-PAGE gradient gels (8–16% acrylamide) were from Bio-Rad. All endonucleases were obtained from New England Biolabs. The synthetic gene encoding NANS ACP1 with codons optimized for expression in *Escherichia coli* was ordered from DNA2.0 Inc. Recombinant Sfp was expressed and purified as previously described (25). NANS module 2+TE was expressed and purified as previously reported (19). Synthetic (±)-2-methyl-3- ketobutyryl-*N*-acetylcysteamine thioester (**1**) (26) as well as the authentic reference standards (2*S*,4*R*)-2,4-dimethyl-5-ketohexanoic acid (**4a**), (2*S*,4*S*)-2,4-dimethyl-5-ketohexanoic acid (**4b**) (19), (2*RS*,4*RS*)-2,4-dimethyl-5-ketohexanoic acid (**4**) (27), and 3,5,6-trimethyl-4-hydroxypyrone (**3**) (28) were each prepared according to the cited literature methods and fully characterized by NMR and GC-MS.

(2RS)-2-methyl-3-ketobutyryl-CoA (2-SCoA)

The (2*RS*)-2-methyl-3-ketobutyryl-CoA (**2-SCoA**) was synthesized as previously described (29). The structure was characterized by ^{1}H and ^{13}C NMR, MALDI-TOF (Supplementary Figure S2) and LC-ESI(+)MS^3 (Figure 3B). The LC-MS^3 analysis was performed using an Agilent Eclipse XDB-C18 column (2.1 mm×150 mm, 3.5 μm). Gradient program: 0–1.5 min, isocratic 95% water + 5% methanol + 0.1% formic acid; 1.5 to 14 min, methanol concentration linearly increased to 65%; 14–15 min, 65 to 100% methanol; 15–20 min, 100% MeOH column rinse; flow rate 200 μL/min. ^{1}H NMR ($CDCl_3$, 400 MHz) δ 0.60 (s, 3H, −C*CH*$_3$), 0.73 (s, 3H, −C*CH*$_3$), 1.17 (s, 3H, −CH*CH*$_3$), 2.13 (s, 3H, −CO*CH*$_3$), 2.28 (t, 2H, *J*=6.8 Hz, HNCO*CH*$_2$), 2.90 (t, 2H, *J*=6.0 Hz, −S*CH*$_2$CH$_2$), 3.20 (t, 2H, *J*=6.0 Hz, −NH*CH*$_2$), 3.30 (t, 2H, *J*=6.4 Hz, −SCH$_2$*CH*$_2$), 3.39 (m, 1H, OH*CH*), 3.68 (m, 1H, H_2O_3PO*CH*), 3.87 (s, 1H, O*CH*), 4.10 (s, 2H, O*CH*$_2$), 4.45 (s, 1H, HO*CH*CO), 6.02 (d, 1H, *J*=6.8 Hz, N*CH*), 8.10 (s, 1H, NH$_2$CN*CH*N), 8.41 (s, 1H, N*CH*N) ^{13}C NMR ($CDCl_3$, 100 MHz) δ 8.04 (C*CH*$_3$), 13.07 (C*CH*$_3$), 15.78 (CH*CH*$_3$), 23.44 (−CO*CH*$_3$), 23.51 (*C*CH3), 30.27 (HNCO*CH*$_2$), 30.35 (−S*CH*$_2$CH$_2$), 33.29 (−NH*CH*$_2$), 33.31 (−SCH$_2$*CH*$_2$), 60.58 (*CH*CH$_3$), 66.84 (POCH$_2$), 68.85 (OHCH), 69.04 (PO*CH*$_2$CH), 69.26 (H_2O_3POCH), 78.74 (POCH$_2$*CH*), 78.86 (HO*CH*CO), 81.38 (NCHO), 113.51, 134.80, 144.30, 147.80, 150.49 (adenine), 168.93 (HN*CO*CH$_2$), 169.67 (HNCOCH), 195.06 (−SCO), 203.88 (*CO*CH$_3$)

Expression and purification of apo-NANS ACP1

Plasmid pXG_NANS_ACP1_5 for expression of *NANS* ACP1 corresponding to the region from T2747 to N2902 of NANS module 1 (20) was constructed by subcloning the synthetic gene optimized for expression in *E. coli* into pET-28a using the appended *NdeI* and *XhoI* restriction sites. Plasmid pXG_NANS_ACP1_5 was transformed by electroporation into *E. coli* BL21(DE3) and the resulting transformant, *E. coli* BL21(DE3)/pXG_NANS_ACP1_5, was grown in LB/kanamycin medium to an OD_{600} 0.6. Protein expression was induced by adding 0.4 mM IPTG and incubating for an additional 20 h at 18 °C. The cells from 2 L of culture were harvested and lysed in 30 mL of lysis buffer (50 mM sodium phosphate, 300 mM NaCl, 1 mM benzamidine, 2 mg/L leupepsin, 2 mg/L pepstatin, 5 mM β-mercaptoethanol, pH 8.0) by two passages through a French pressure cell at 10,000 psi. The resulting cell lysate containing N-terminal His_6-tagged *apo*-NANS ACP1 was centrifuged at 53,000*g* to remove cell debris and the supernatant was mixed with 5 mL of Ni-NTA resin. After gentle shaking at 4 °C for 1 h, the slurry was transferred to a fritted column (I.D. 1.5 cm), washed with 5 col. vol. of wash buffer (50 mM sodium phosphate, 300 mM NaCl, 30 mM imidazole, 1 mM β-mercaptoethanol, pH 8.0) and eluted with 5 col. vol. of elution buffer (50 mM sodium phosphate, 300 mM NaCl, 250 mM imidazole, 1mM β-mercaptoethanol, pH 8.0). The protein-containing eluant was concentrated with 10K MWCO centrifugal filters and further purified by FPLC gel filtration chromatography with a HiLoad 16/60 Superdex 200 column from Amersham Biosciences (50 mM sodium phosphate, 350 mM NaCl, 10% glycerol, pH 6.5). The purified protein fractions were pooled, concentrated and aliquots were flash-frozen in liquid nitrogen and stored at −80 °C until use. The purity and MW of His_6-tag-*apo*-ACP1 were confirmed by SDS PAGE and LC-ESI(+)-MS (Supplementary Figure S3).

Chemoenzymatic preparation of 2-methyl-3-ketobutyryl-ACP1 (2-ACP1)

In 5 mL sodium phosphate buffer (50 mM sodium phosphate, 350 mM NaCl, 300 μM TCEP, 10 mM $MgCl_2$, pH 6.40), *apo*-NANS ACP1 (46 μM) was incubated with Sfp PPTase (5.8 μM) and 2-methyl-3- ketobutyryl-CoA (**2-SCoA**) (138 μM) for 45 min in a 30 °C water bath (25, 30). The mixture was concentrated to 2 mL in a 10 kDa centrifugal filter and purified by FPLC gel filtration chromatography with a HiLoad 16/60 Superdex 200 column from Amersham Biosciences (buffer: 50 mM sodium phosphate, 350 mM NaCl, pH 6.40). The pooled fractions were then concentrated to 250 μL and the concentration of **2-ACP1** was determined to be 450 μM by Bradford assay. The sample was analyzed by LC-ESI(+)MS^3 (Figure 3C).

NANS Module 2+TE activity assays with 2-methyl-3-ketobutyryl-ACP1 (2-ACP1)

The assays used with ACP1-bound substrate **2-ACP1**, were based on those previously described for incubations with **2-SNAC** (19), which were also repeated in order to allow direct comparisons of reaction product distributions.

Radio TLC-Phosphorimaging

In a total volume of 50 μL of assay buffer (250 mM sodium phosphate, 1 mM EDTA, 2.5 mM TCEP, 5% glycerol, pH 7.2), NANS module 2+TE (2 μM) was pre-incubated with NADPH (5 mM) for 30 min. Then 2-methyl-3-ketobutyryl-ACP1 (**2- ACP1**, 60 μM, from 450 μM stock) and [2-^{14}C]methylmalonyl-CoA (0.74 mCi/mmol, 0.2 mM, from a 2 mM stock in 10 mM HCl) were added in three aliquots every 15 min. The reaction was allowed to stand 2 h and then quenched by addition of 15 μL of 2 M HCl, followed by extraction with EtOAc (3×250 μL). The organic solvent was removed by Speed-Vac and the crude organic extract was resuspended in 3×20 μL of EtOAc and analyzed by TLC (silica gel, 1:1 Et_2O/CH_2Cl_2+0.1% AcOH). Radio-TLC results were visualized by phosphorimaging

(Figure 4A). Formation of the expected products was confirmed by comparison with synthetic 3,5,6-trimethyl-4-hydroxypyrone **(3**) and (2*S*,4*R*)-2,4-dimethyl-5-ketohexanoic acid (**4a**). (The TLC conditions cannot resolve the diastereomers **4a** and **4b**.)

LC-ESI(+)MS^2 analysis of enzyme-generated 3 and chiral GC-EI(+)MS analysis of enzyme-generated 4a

The above phosphorimaging analysis indicated pyrone **3** was also formed along with **4a** in the incubation with NADPH. Thus, the enzyme-generated pyrone **3** and the saturated triketide acid **4a** could each be isolated from the same TLC plate. A 500-μL-scale incubation of NANS module 2+TE (2 μM) was carried out as described above with ACP-bound substrate, **2-ACP1** and [2-^{14}C]methylmalonyl-CoA (0.25 mCi/mmol, 0.2 mM) in the presence of 5 mM NADPH. The reaction was run for 2 h and then quenched by addition of 150 μL of 2 M HCl followed by extraction with EtOAc (7×1 mL). The organic solvent was evaporated and the crude organic extract was resuspended in 3×20 μL of EtOAc and separated by TLC (1/1 Et_2O/CH_2Cl_2 + 0.1 % AcOH). Radio-TLC results were visualized by phosphorimaging to locate the band corresponding to the enzyme-generated pyrone **3** and the enzyme-generated triketide acid **4a**. The silica gel containing pyrone **3** was scraped off, extracted with 3×3 mL EtOAc and the solvent removed by Speedvac. The residue was dissolved in 200 μL acetonitrile and **3** was analyzed by LC-ESI(+)MS^2 (Figure S3). Enzyme-generated **4a** was also scraped off and extracted with 3×3 mL EtOAc. After evaporation of solvent by rotary evaporator, the residue was dissolved in 100 μL of MeOH and treated with 15 μL of trimethylsilyldiazomethane (2 M in hexane) at r.t. for 30 min to generate the corresponding methyl esters, followed by AcOH quench. The methanolic solution was then directly analyzed by chiral GC-EI(+)-MS (Figure 4).

Steady-state kinetics for incubation of 2-methyl-3-ketobutyryl-ACP1 (2-ACP1) with NANS module 2+TE

The steady-state parameters for the NANS module 2+TE-catalyzed formation of pyrone **3** were determined in the absence of NADPH, as previously described (19). The methodology was based on that previously used to characterize other recombinant PKS modules (31). Preliminary experiments established that the enzyme-catalyzed reaction was linear over a period of 90 min. All single-point kinetic assays were therefore based on an incubation time of 45 min at 30 °C. For determination of the steady-state kinetic parameters for methylmalonyl- CoA, 10.8 μg of recombinant NANS module 2+TE (0.044 nmol, 4 μL of a solution of 2.7 μg/μL, final concentration 0.88 μM) were mixed with 29.9 μL of assay buffer (250 mM sodium phosphate, 1 mM EDTA, 2.5 mM TCEP, 5% glycerol, pH 7.2). Then 11.1 μL of ACP-bound substrate **2-ACP1** (450 μM, final concentration **2**, 100 μM) was added. The concentration of **2-ACP1** was not corrected for the <20% *holo*-ACP1 that is present in the sample, as determined by LC-ESI(+)-MS (Figure 3C.i). Variable concentrations of [2-^{14}C]methylmalonyl-CoA (0.74 mCi/mmol, 5 μL, final concentrations of 0.0625 mM, 0.125 mM, 0.25 mM, 0.5 mM and 1 mM) were then added to bring the total volume to 50 μL and the incubation was continued for 45 min. The reaction was quenched with 15 μL of 2 M HCl and extracted with 4×300 μL EtOAc. The organic layer was then concentrated by Speedvac and spotted onto a flexible silica gel TLC plate along with reference samples of unlabeled **3**. The TLC plate was developed with 1:1 Et_2O/CH_2Cl_2 + 0.1% acetic acid and then analyzed by phosphorimaging. The system was precalibrated by applying serial dilutions of [2-^{14}C]methylmalonyl-CoA to a reference plate. After exposure, the plate was stained with iodine to visualize the products and locate the pyrone product **3**. Kinetic constants were calculated using the program Kaleidagraph 4.0 to fit the data to the Michaelis-Menten equation. Reported standard deviations in the steady-state kinetic parameters represent the calculated statistical errors in the non-linear, least squares regression analysis. For determination of the steady-state kinetic parameters for 2-methyl-3-

ketobutyryl- ACP1 (**2-ACP1**), the procedure was the same, with the methylmalonyl-CoA concentration fixed at 1 mM and variable **2-ACP1** (6.25 μM, 12.5 μM, 25 μM, 50 μM, and 100 μM). Since each set of kinetic measurements was performed at sub-saturating concentrations of the fixed **2-ACP1** or [2-^{14}C]methylmalonyl-CoA co-substrate, the k_{cat}(apparent) values were corrected to give an extrapolated to k_{cat}(actual), using the Michaelis-Menten relationship $k_{cat}(app) = k_{cat}(actual)\cdot\{[A]/(K_m + [A])\}$ where [A] is the concentration of the fixed-co-substrate and K_m is the *Michaelis* constant determined for the fixed co-substrate in the complementary kinetic experiments when the other co-substrate concentration was held constant.

RESULTS AND DISCUSSION

Preparation of (2RS)-2-methyl-3-ketobutyryl-NANS ACP1 (2-ACP1)

To obtain recombinant NANS ACP1, a synthetic gene optimized for expression in *E. coli* and corresponding to the region from T2747 to N2902 of NanA1 was first subcloned into pET-28a using appended *NdeI* and *XhoI* restriction sites. The resulting plasmid pXG_NANS_ACP1_5 was transformed into *E. coli* BL21(DE3) and the resulting transformant was used for production of His_6-tag-*apo*-ACP1 which was obtained in a yield of 14 mg/L culture and 95% purity after Ni-NTA immobilized metal ion affinity chromatography and gel filtration, The MW was determined by LC-ESI(+)-MS as 18,663 Da (calc, 18,659, Supplementary Figure S3). The requisite (2*RS*)-2-methyl-3- ketobutyryl-CoA (**2-SCoA**) was prepared from ethyl 2-methylacetoacetate as previously described (29) (Figure 3A) and the structure was verified by MALDI-TOF MS (Supplementary Figure S2) and LC-ESI(+)-MS-MS (Figure 3B) as well as ^{1}H and ^{13}C NMR. Using Sfp phosphopantetheinyl transferase (PPTase) (25, 30), the phosphopantetheinyl unit of (*2RS*)-*2*-methyl-3-ketobutyryl-CoA (**2-SCoA**) was fused to *apo*-NANS ACP1 to afford (*2RS*)-2-methyl- 3-ketobutyryl-ACP1 (**2-ACP1**). LC-ESI(+)-MS-MS-MS analysis confirmed the formation of 2-methyl-3-ketobutyryl-ACP1 (**2-ACP1**) (78%, $[M]^{23+}$ *m/z* 831.41; calcd $[M]^{+}$ 19,100; [predicted MW 19101]) (Figure 3C). The MS^2 spectrum of **2-ACP1** exhibited the characteristic phosphopantetheinate (PPant) ejection fragment (*m/z* 359.26) carrying the 2-methyl-3- ketobutyryl moiety, while the corresponding MS^3 spectrum displayed characteristic fragments at *m/z* 257.18 and 261.27, resulting from further collision-induced cleavage of the pantoate moiety and the thioester bond, respectively (32, 33) (Figure 3C), in close agreement with the corresponding MS^2 and MS^3 spectra of 2-methyl-3-ketobutyryl-CoA (**2-SCoA**) (Figure 3B).

Enzymatic formation of 3,5,6-trimethyl-4-hydroxypyrone (3)

Incubation of NANS module 2+TE with (*2RS*)-*2*-methyl-3-ketobutyryl-ACP1 (**2-ACP1**) and [2-^{14}C]methylmalonyl-CoA in the absence of NADPH for 2 h and analysis of the resulting concentrated crude organic extract by radio-TLC phosphorimaging gave as the major product pyrone **3** (R_f 0.5), identical to synthetic **3** (Figures 2B-a and 4A). The result was confirmed by LC-ESI(+)-MS-MS analysis of TLC-purified **3** obtained from a 500 μL-scale incubation of NANS module 2+TE with **2-ACP1** and [2-^{14}C]methylmalonyl-CoA (Supplementary Figure S4). The MS spectrum (ret. time 5.08 min, *m/z* 155) and MS^2 spectrum (m/z 81, 109 and 127) of enzyme-generated **3** were identical to those of synthetic 3,5,6-trimethyl-4-hydroxypyrone (**3**). Steady-state kinetic analysis (45 min incubation) carried out at a fixed concentration of **2-ACP1** (100 μM) and variable concentrations of methylmalonyl-CoA gave a k_{cat}(app) of 2.4±0.3 min^{-1} and a K_m (MM-CoA) of 0.25±0.08 mM (Supplementary Figure S5). When **2-ACP1** was the variable substrate and the methylmalonyl- CoA concentration was fixed at 1 mM, the k_{cat}(app) was 3.5±0.7 min^{-1} and K_m(**2-ACP1**) was 66±26 μM (Supplementary Figure S5). Correction for the sub-saturating concentrations of each fixed co-substrate using the Michaelis-Menten equation gave a

calculated k_{cat}(actual) of 4.4±0.9 min^{-1}. Comparison with the corresponding steady state kinetic parameters of the diffusive substrate (*2RS*)-2-methyl-3-ketobutyryl-SNAC (**2-SNAC**) (19) obtained under identical conditions indicated that while k_{cat}(actual) for ACP1-bound substrate **2-ACP1** had increased a modest 8-fold from 0.55 min^{-1} (**2-SNAC**), the observed K_m for **2-ACP1** was ~300-fold lower than the K_m of 19 mM for **2-SNAC** measured under the same conditions, resulting in a net ~2300-fold increase in k_{cat}/K_m from 29 $min^{-1}M^{-1}$ (**2-SNAC**) to 6.7 × 10^4 $min^{-1}M^{-1}$ (**2-ACP1**). NANS module 2+TE thus has a strong kinetic preference for the ACP-bound substrate **2-ACP1** over the diffusive thioester substrate analogue **2-SNAC**. Since the measured k_{cat}/K_m of NANS module 2+TE is intrinsically a function of only those kinetic events up to and including the first irreversible biochemical step, this kinetic parameter directly reflects the catalytic specificity of the KS2 domain (6).

Stereospecific formation of (2S,4R)-2,4-dimethyl-5-ketohexanoate (4a) using ACP-bound substrate

Incubation of NANS module 2+TE with (*2RS*)-2-methyl-3-ketobutyryl-ACP1 (**2-ACP1**) in the presence of 0.25 mM [2-^{14}C]methylmalonyl-CoA and 5 mM NADPH followed by analysis of the crude organic extract by radio-TLC phosphorimaging demonstrated the formation of triketide acid **4** (R_f 0.6) accompanied by pyrone **3**, the latter formed by premature TE-catalyzed release of the initially-formed chain elongation intermediate, as previously observed for the corresponding **2-SNAC** analogue. (Figures 2 and 4A) (19). The enzyme-generated sample of **4** was derivatized with $TMSCHN_2$ and analyzed by chiral GCEI(+)- MS (19). The enzymatic reaction product corresponded exclusively to (2*S*,4*R*)-**4a-Me**, the methyl ester of the native (2*S*,4*R*)-2,4-dimethyl-5-ketohexanoic acid (**4a**), ret. time 5.37 min, identical by direct comparison in TIC, XIC, and SIM modes (*m/z* 88) with synthetic methyl ester **4a-Me** in both ret. time and MS fragmentation pattern (Figures 2B–b and 4 and Supplementary Figure S4C). Neither the diastereomeric (2*S*,4*S*)-**4b-Me** nor either of the remaining two diastereomers of **4-Me** could be detected, in contrast to the 5:3 mixture of **4a-Me** and **4b-Me** that was generated using the diffusive SNAC substrate analogue **2-SNAC**. The KS2 domain of NANS module 2 is therefore completely stereospecific with respect to translocation of the correct epimer of ***2*-ACP1**, the NANS ACP1-bound mixture of the natural (2*S*)-2-methyl-3- ketobutyryl substrate and the epimeric (2*R*)-diastereomer (Figure 2B–b).

The NanA1 protein that normally supplies the substrate for NANS module 2 is comprised of both a loading KS^Q-AT-ACP tridomain and the first polyketide chain extension module, NANS module 1 (20). The loading tridomain provides the acetyl-ACP_L starter unit, derived from malonyl-CoA, which then serves as the primer for the KS1 domain of NANS module 1. NANS KS1-catalyzed decarboxylative condensation reaction with (2*S*)-methylmalonyl-ACP1 is expected to proceed with inversion of configuration to afford (2*R*)-2-methyl-3-ketobutyryl- SACP1 (7, 16), NANS module 1 also harbors a reductively inactive KR^0 domain, analogous to that found in the ketone-forming modules of numerous macrolide synthases including DEBS module 3 (1, 34–36).

The initially formed (2*R*)-2-methyl-3-ketobutyryl-SACP1 diastereomer must be converted at some stage to the epimeric (2*S*)-2-methyl-3-ketobutyryl stereoisomer that serves as the electrophilic substrate for NANS KS2. Simple buffer-catalyzed interconversion of the (2*R*)- and (2*S*)-2-methyl-3-ketobutyryl epimers can be ruled out since the established background epimerization rate of <0.01 min^{-1} for ACP-bound substrate is considerably slower than the typical rate of KS-catalyzed condensation (>1–4 min^{-1}) which is itself the rate-determining step for each module (7, 16). The KS2 domain thus must cleanly discriminate between the two epimers of the ACP1-bound ketodiketide substrate, resulting in priming of KS2 by only (2*S*)- 2-methyl-3-ketobutyryl-ACP1 (**2-ACP1**). *Epimerization of the 2-methyl group must*

therefore precede covalent attachment of the electrophilic 2-methyl-3-ketoacyl substrate to the active site Cys of the downstream KS domain. The requisite epimerase activity may in principle either reside in NANS module 1, possibly associated with the reductively inactive $KR1^0$ domain (37), or it may be associated with the KS2 domain of NANS module 2. In the latter case, KS2 would have to interconvert the epimers of the KS2-bound 2-methyl-3-ketobutyryl substrate *prior to* the condensation reaction. Translocation of the 2-methyl-3-ketobutyryl displaces the original thioester, be it the natural ACP1-SH or the *N*-acetylcysteamine analogue. Once the transesterification of the active site cysteine of the KS2 domain has occurred, there is thus no longer any distinction between the origin of respective electrophilic 2-methyl-3-ketobutyryl units. Epimerization after acylation of the active site cysteine by the incorrect (2*R*)-epimer is firmly excluded by the previously observed lack of discrimination between the two epimers of 2- methyl-3-ketobutyryl-SNAC that results in formation of a 5:3 mixture of the diastereomeric triketide acids **4a** and **4b** from the diffusive substrate (±)-**2-SNAC** (19). The KS2 domain therefore serves as a gatekeeper that translocates only the natural ACP1-bound (2*S*)-2-methyl-3- ketoacylbutyryl substrate and rejects the corresponding (2*R*)-2-methyl-3-ketoacyl diastereomer that would be initially generated by the KS1 domain of the upstream module. The observed stereospecificity for diketide translocation by the NANS KS2 domain presumably reflects specific interactions with the partner ACP1 domain carrying the diketide substrate. These essential interactions are apparently absent in the diffusive substrate SNAC substrate analogue **2-SNAC**.

Interestingly modules 3 of both DEBS and picromycin synthase (PICS) also harbor a reductively inactive KR^0 domain that has been suggested to have an intrinsic methyl-epimerase activity (37). This epimerase activity would facilitate the conversion of ACP3-bound (2*R*)-2- methyl-3-ketoacyl tetraketide intermediates, initially generated by the corresponding DEBS and PICS KS3-mediated condensation reactions, to the epimeric ACP3-bound (2*S*)-2-methyl-3- ketoacyl tetraketides, prior to translocation of the electrophilic product to the respective downstream PICS or DEBS KS4 domains. Notably, both DEBS and PICS module 4 also mediate the full set of reductive β-ketoacyl-ACP KR-, DH-, and ER-catalyzed chain processing reactions so as to generate a fully reduced polyketide chain elongation product, analogous to the catalytic action of NANS module 2 (Figure S1).

Significance

The ability of the NANS KS2 domain to distinguish between the (2*S*)- and (2*R*)- epimers of its natural 2-methyl-3-ketobutyryl-ACP1 substrate depends critically on the tethering of the substrate to an ACP domain. This is most likely due to specific KS–ACP interactions, since there is only a modest 5:3 discrimination in favor of the diffusive (2*S*)-2-methyl-3-ketobutyryl-SNAC analogue. It is unlikely that the pantetheinate residue alone could account for the dramatic increase in stereospecificity in NANS KS2-catalyzed chain translocation as well as the observed 2300-fold increase in k_{cat}/K_m observed for **2-ACP1**. The requisite epimerization of the endogenously generated, ACP-bound (2*R*)-2-methyl-3-keto-diketide must occur prior to chain translocation and processing by the downstream KS2 domain, which is itself completely stereoselective for the correct epimer of the ACP-bound chain elongation substrate. Although it has previously been reported that the catalytic efficiency of individual DEBS modules, as measured by the observed k_{cat}/K_m, is enhanced 1000-fold by using ACP-bound diketide substrates in place of the SNAC thioester analogues, the use of such ACP-bound diketides did not alter the observed substrate stereospecificity of the DEBS KS domains (4, 5).

In addition to nanchangmycin (also known as dianemycin), many polyether natural products, including lenoremycin, monensin, laidlomycin, nigericin, grisorixin, mutalomycin, septamycin, and carriomycin have identical dimethyltetrahydropyranyl moieties distal to

their carboxyterminal ends, each of which is derived from a common (2*S*,4*R*)-2,4-dimethyl-5-ketohexanoyl triketide precursor (38) (Supplemental Figure S1). Indeed, the first nine modules of the nanchangmycin, monensin, and nigericin PKS clusters show a striking similarity in both their overall modular organization and the specific domain content, particularly the presence of an inactive KR^0 domain in module 1, as well as a discrete, fully reductive module 2 (39). It is therefore evident that the observed stereospecific interaction of NANS module 2 with the ACP1- bound 2-methyl-3-ketobutyryl diketide is directly relevant to the biochemical action of a wide range of polyether synthases. These results can also account for the stereochemistry of formation of the (2*S*,4*R*)-2,4-dimethyl-5-ketohexanoate moiety found at the carboxyl termini of both nanchangmycin and lenoremycin. Finally, these results may also account for the generation of the common (6*S*,8*S*)-6,8-dimethyl-9-keto substitution pattern that is present in erythromycin and numerous other macrolides, as summarized by the well-known Celmer's Rules (40, 41) and exemplified by the macrolide aglycones 10-deoxymethynolide, 6-deoxyerythronolide B, and tylactone (Figure S1).

Supplementary Material

Refer to Web version on PubMed Central for supplementary material.

Acknowledgments

We thank Dr. Dongqing Zhu for her help and advice with the cloning experiments, Dr. Tun-Li Shen for assistance with mass spectrometry, and Dr. Russell Hopson for assistance with NMR. We also thank Prof. Chaitan Khosla of Stanford University for critical comments on the manuscript.

References

1. Hopwood, DA. Complex enzymes in microbial natural product biosynthesis, part B: polyketides, aminocoumarins and carbohydrates. Vol. 459. Academic Press; 2009. Methods in Enzymology.
2. Smith S, Tsai SC. The type I fatty acid and polyketide synthases: a tale of two megasynthases. Nat Prod Rep. 2007; 24:1041–1072. [PubMed: 17898897]
3. Berg, JM.; Tymoczko, JL.; Stryer, L. Biochemistry. 6. W. H. Freeman; New York: 2007.
4. Wu N, Cane David E, Khosla C. Quantitative analysis of the relative contributions of donor acyl carrier proteins, acceptor ketosynthases, and linker regions to intermodular transfer of intermediates in hybrid polyketide synthases. Biochemistry. 2002; 41:5056–5066. [PubMed: 11939803]
5. Wu N, Tsuji SY, Cane DE, Khosla C. Assessing the balance between protein-protein interactions and enzyme- substrate interactions in the channeling of intermediates between polyketide synthase modules. J Am Chem Soc. 2001; 123:6465–6474. [PubMed: 11439032]
6. Wu J, Kinoshita K, Khosla C, Cane DE. Biochemical analysis of the substrate specificity of the beta-ketoacyl-acyl carrier protein synthase domain of module 2 of the erythromycin polyketide synthase. Biochemistry. 2004; 43:16301–16310. [PubMed: 15610024]
7. Khosla C, Tang Y, Chen AY, Schnarr NA, Cane DE. Structure and mechanism of the 6-deoxyerythronolide B synthase. Annu Rev Biochem. 2007; 76:195–221. [PubMed: 17328673]
8. Tang Y, Chen AY, Kim CY, Cane DE, Khosla C. Structural and mechanistic analysis of protein interactions in module 3 of the 6-deoxyerythronolide B synthase. Chem Biol. 2007; 14:931–943. [PubMed: 17719492]
9. Tang Y, Kim CY, Mathews II, Cane DE, Khosla C. The 2.7-Å crystal structure of a 194-kDa homodimeric fragment of the 6-deoxyerythronolide B synthase. Proc Natl Acad Sci U S A. 2006; 103:11124–11129. [PubMed: 16844787]
10. Maier T, Jenni S, Ban N. Architecture of mammalian fatty acid synthase at 4.5 Å resolution. Science. 2006; 311:1258–1262. [PubMed: 16513975]
11. Leibundgut M, Maier T, Jenni S, Ban N. The multienzyme architecture of eukaryotic fatty acid synthases. Curr Opin Struct Biol. 2008; 18:714–725. [PubMed: 18948193]

12. Maier T, Leibundgut M, Ban N. The crystal structure of a mammalian fatty acid synthase. Science. 2008; 321:1315–1322. [PubMed: 18772430]
13. Kapur S, Chen AY, Cane DE, Khosla C. Molecular recognition between ketosynthase and acyl carrier protein domains of the 6-deoxyerythronolide B synthase. Proc Natl Acad Sci U S A. 2010; 107:22066–22071. [PubMed: 21127271]
14. Charkoudian LK, Liu CW, Capone S, Kapur S, Cane DE, Togni A, Seebach D, Khosla C. Probing the interactions of an acyl carrier protein domain from the 6- deoxyerythronolide B synthase. Protein Sci. 2011; 20:1244–1255. [PubMed: 21563224]
15. Castonguay R, Valenzano CR, Chen AY, Keatinge-Clay A, Khosla C, Cane DE. Stereospecificity of ketoreductase domains 1 and 2 of the tylactone modular polyketide synthase. J Am Chem Soc. 2008; 130:11598–11599. [PubMed: 18693734]
16. Valenzano CR, Lawson RJ, Chen AY, Khosla C, Cane DE. The biochemical basis for stereochemical control in polyketide biosynthesis. J Am Chem Soc. 2009; 131:18501–18511. [PubMed: 19928853]
17. Valenzano CR, You YO, Garg A, Keatinge-Clay A, Khosla C, Cane DE. Stereospecificity of the dehydratase domain of the erythromycin polyketide synthase. J Am Chem Soc. 2010; 132:14697–14699. [PubMed: 20925342]
18. Keatinge-Clay A. Crystal structure of the erythromycin polyketide synthase dehydratase. J Mol Biol. 2008; 384:941–953. [PubMed: 18952099]
19. Guo X, Liu T, Valenzano CR, Deng Z, Cane DE. Mechanism and stereospecificity of a fully saturating polyketide synthase module: nanchangmycin synthase module 2 and its dehydratase domain. J Am Chem Soc. 2010; 132:14694–14696. [PubMed: 20925339]
20. Sun Y, Zhou X, Dong H, Tu G, Wang M, Wang B, Deng Z. A complete gene cluster from *Streptomyces nanchangensis* NS3226 encoding biosynthesis of the polyether ionophore nanchangmycin. Chem Biol. 2003; 10:431–441. [PubMed: 12770825]
21. Liu T, Cane DE, Deng Z. The enzymology of polyether biosynthesis. Methods Enzymol. 2009; 459:187–214. [PubMed: 19362641]
22. Sambrook, J.; Fritsch, EF.; Maniatis, T. Molecular Cloning, A Laboratory Manual. 2. Cold Spring Harbor Laboratory Press; Cold Spring Harbor, NY: 1989.
23. Bradford M. A rapid and sensitive method for the quantitation of microgram quantitites of protein utilizing the principle of protein-dye binding. Anal Biochem. 1976; 72:248–254. [PubMed: 942051]
24. Laemmli UK. Cleavage of structural proteins during the assembly of the head of bacteriophage T4. Nature (London). 1970; 227:680–685. [PubMed: 5432063]
25. Quadri LE, Weinreb PH, Lei M, Nakano MM, Zuber P, Walsh CT. Characterization of Sfp, a *Bacillus subtilis* phosphopantetheinyl transferase for peptidyl carrier protein domains in peptide synthetases. Biochemistry. 1998; 37:1585–1595. [PubMed: 9484229]
26. Weissman KJ, Bycroft M, Cutter AL, Hanefeld U, Frost EJ, Timoney MC, Harris R, Handa S, Roddis M, Staunton J, Leadlay PF. Evaluating precursordirected biosynthesis towards novel erythromycins through in vitro studies on a bimodular polyketide synthase. Chem Biol. 1998; 5:743–754. [PubMed: 9862800]
27. Mukherjee S, Nasipuri D. Heterocyclic steroids: Part IV - Synthesis of (±)- 3-methoxy-11α±-methyl-6,15-diazaestra-1,3,5,7,9,14-hexaene and some related hydrophenanthridinones. Indian J Chem, Sect B. 1984; 23B:193–198.
28. Shimamura H, Sunazuka T, Izuhara T, Hirose T, Shiomi K, Omura S. Total synthesis and biological evaluation of verticipyrone and analogues. Org Lett. 2007; 9:65–67. [PubMed: 17192086]
29. Haapalainen AM, Merilainen G, Pirila PL, Kondo N, Fukao T, Wierenga RK. Crystallographic and kinetic studies of human mitochondrial acetoacetyl-CoA thiolase: The importance of potassium and chloride ions for its structure and function. Biochemistry. 2007; 46:4305–4321. [PubMed: 17371050]
30. Weinreb PH, Quadri LE, Walsh CT, Zuber P. Stoichiometry and specificity of in vitro phosphopantetheinylation and aminoacylation of the valine-activating module of surfactin synthetase. Biochemistry. 1998; 37:1575–1584. [PubMed: 9484228]

31. Wu N, Kudo F, Cane DE, Khosla C. Analysis of the molecular recognition features of individual modules derived from the erythromycin polyketide synthase. J Am Chem Soc. 2000; 122:4847–4852.
32. Dorrestein PC, Bumpus SB, Calderone CT, Garneau-Tsodikova S, Aron ZD, Straight PD, Kolter R, Walsh CT, Kelleher NL. Facile detection of acyl and peptidyl intermediates on thiotemplate carrier domains via phosphopantetheinyl elimination reactions during tandem mass spectrometry. Biochemistry. 2006; 45:12756–12766. [PubMed: 17042494]
33. Meluzzi D, Zheng WH, Hensler M, Nizet V, Dorrestein PC. Topdown mass spectrometry on low-resolution instruments: characterization of phosphopantetheinylated carrier domains in polyketide and non-ribosomal biosynthetic pathways. Bioorg Med Chem Lett. 2008; 18:3107–3111. [PubMed: 18006314]
34. Donadio S, Staver MJ, Mcalpine JB, Swanson SJ, Katz L. Modular organization of genes required for complex polyketide biosynthesis. Science. 1991; 252:675–679. [PubMed: 2024119]
35. Donadio S, Katz L. Organization of the enzymatic domains in the multifunctional polyketide synthase involved in erythromycin formation in Saccharopolysporaerythraea. Gene. 1992; 111:51–60. [PubMed: 1547954]
36. Cortes J, Haydock SF, Roberts GA, Bevitt DJ, Leadlay PF. An unusually large multifunctional polypeptide in the erythromycin-producing polyketide synthase of Saccharopolyspora erythraea. Nature. 1990; 348:176–178. [PubMed: 2234082]
37. Zheng J, Keatinge-Clay A. Structural and functional analysis of C2-type ketoreductases from modular polyketide synthases. J Mol Biol. 2011; 410:105–117. [PubMed: 21570406]
38. Cane DE, Celmer WD, Westley JW. A unified stereochemical model of polyether structure and biogenesis. J Am Chem Soc. 1983; 105:3594–3600.
39. Harvey BM, Mironenko T, Sun Y, Hong H, Deng Z, Leadlay PF, Weissman KJ, Haydock SF. Insights into polyether biosynthesis from analysis of the nigericin biosynthetic gene cluster in *Streptomyces* sp. DSM4137. Chem Biol. 2007; 14:703–714. [PubMed: 17584617]
40. Celmer WD. A configurational model for macrolide antibiotics. J Am Chem Soc. 1965; 87:1801–1802. [PubMed: 14289343]
41. Celmer WD. Stereochemical problems in macrolide antibiotics. Pure Appl Chem. 1971; 28:413–453. [PubMed: 4947320]

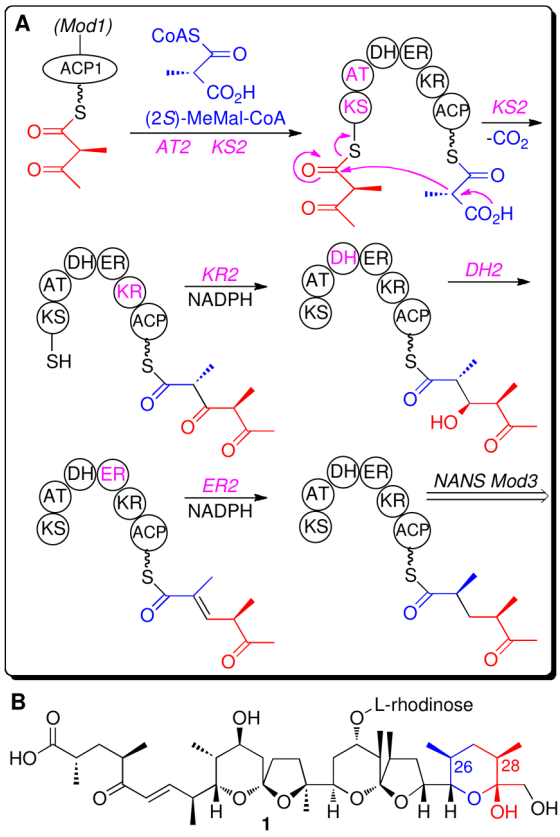

Figure 1.

Early steps of nanchangmycin biosynthesis. A. Polyketide chain elongation and ketoreduction-dehydration-enoylreduction catalyzed by nanchangmycin synthase module 2 (NANS module 2). The acyltransferase (AT2) domain loads the (2*S*)-methylmalonyl chain extension unit onto the ACP of NANS module 2 while the 2-methyl-3-ketobutyryl unit donated by NANS module 1 is translocated by ketosynthase catalyzed self-acylation of the active site cysteine of KS2. Following ketoreduction (KR2), *syn*-dehydration (DH2), and enoylreduction (ER2), the resulting (2*S*,4*R*)-2,4-dimethyl-5-ketohexanoyl product is again translocated to the KS3 domain of NANS module 3 to initiate the next round of polyketide chain elongation and functional group modification. Substructures in red are derived from the electrophilic (*2S*)-*2*- methyl-3-ketobutyryl unit while substructures in blue are derived from (2*S*)-methylmalonyl- CoA. The squiggly bond from the ACP domain to the thioester represents the attached phosphopantetheinyl prosthetic group. B. Polyether nanchangmycin (**1**).

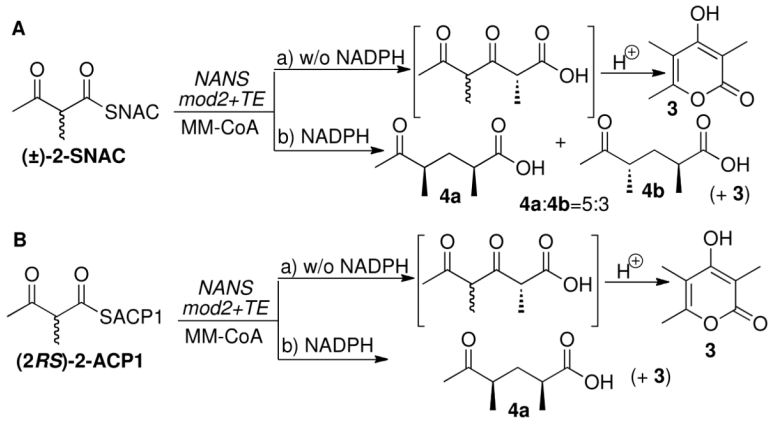

Figure 2.
Incubation of diffusive **2-SNAC** and ACP-bound **2-ACP1** substrates with NANS module 2+TE.

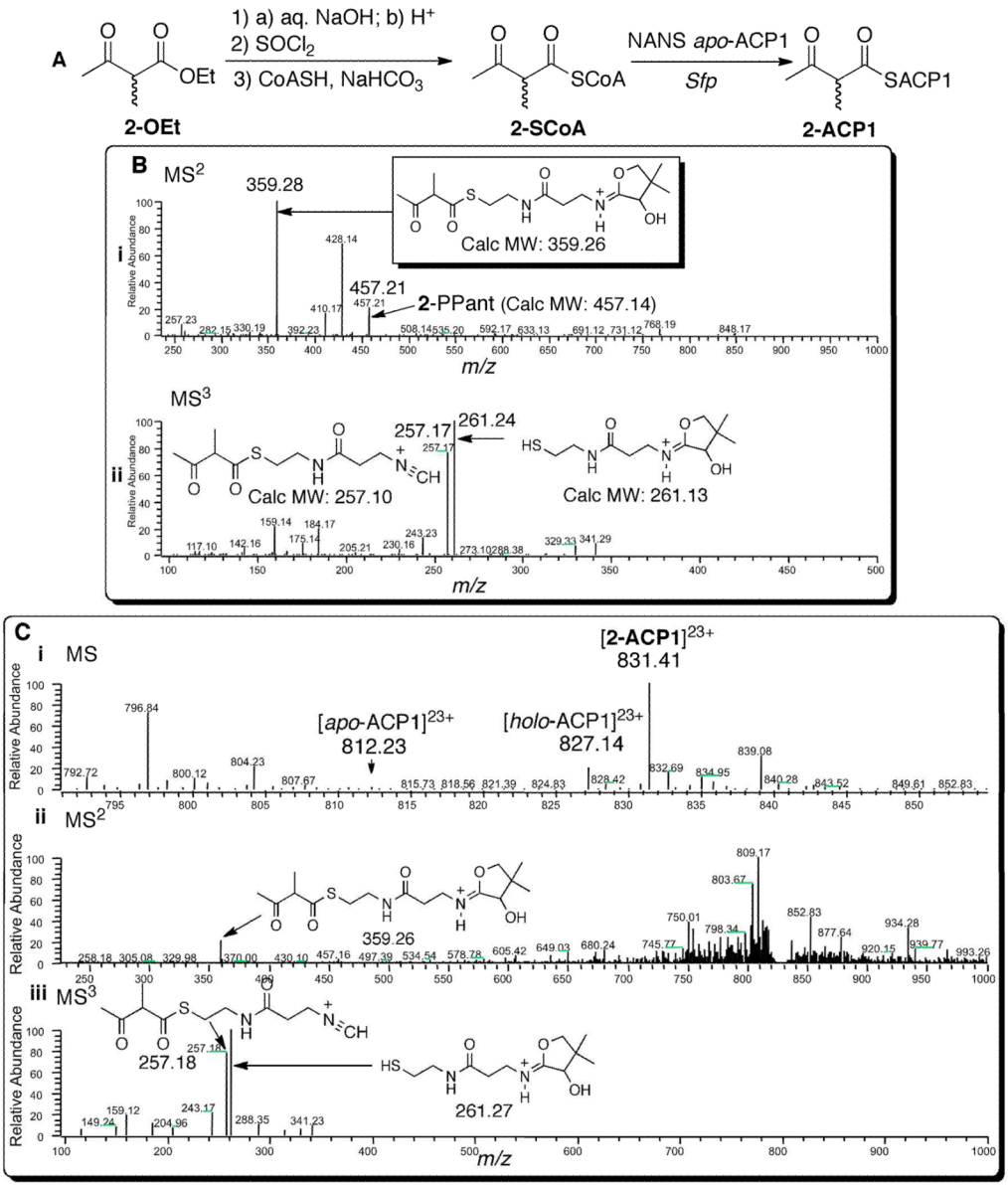

Figure 3.

Chemoenzymatic preparation and LC-ESI(+)-MS characterization of **2-ACP1**. A. Preparation of **2-SCoA** and **2-ACP1**. B, LC-ESI(+)-MS-MS-MS analysis of 2-methyl-3-ketobutyryl-CoA (**2-SCoA**). i, MS^2 fragmentation of **2-SCoA** showing the pPant ejection ion at *m/z* 359.26 and the corresponding phosphorylated pantetheine ejection fragment at *m/z* 457.21; ii, MS^3 fragmentation of pPant ejection ion at *m/z* 359.26, showing collisionally induced fragment ions at *m/z* 261.27 due to loss of 2-methyl-3-ketobutyryl moiety and *m/z* 257.17, due to cleavage of the pantoate moiety. C. LC-ESI(+)-MS-MS-MS analysis of **2-ACP1**. i. ESI(+)-MS, showing $[M]^{23+}$ ion *m/z* 831.41; ii. MS^2 of $[M]^{23+}$ ion *m/z* 831.40, showing pPant ejection ion at *m/z* 359.26; iii. MS^3 of Ppant ejection ion, showing collisionally induced fragment ions at *m/z* 261.27 and 257.18.

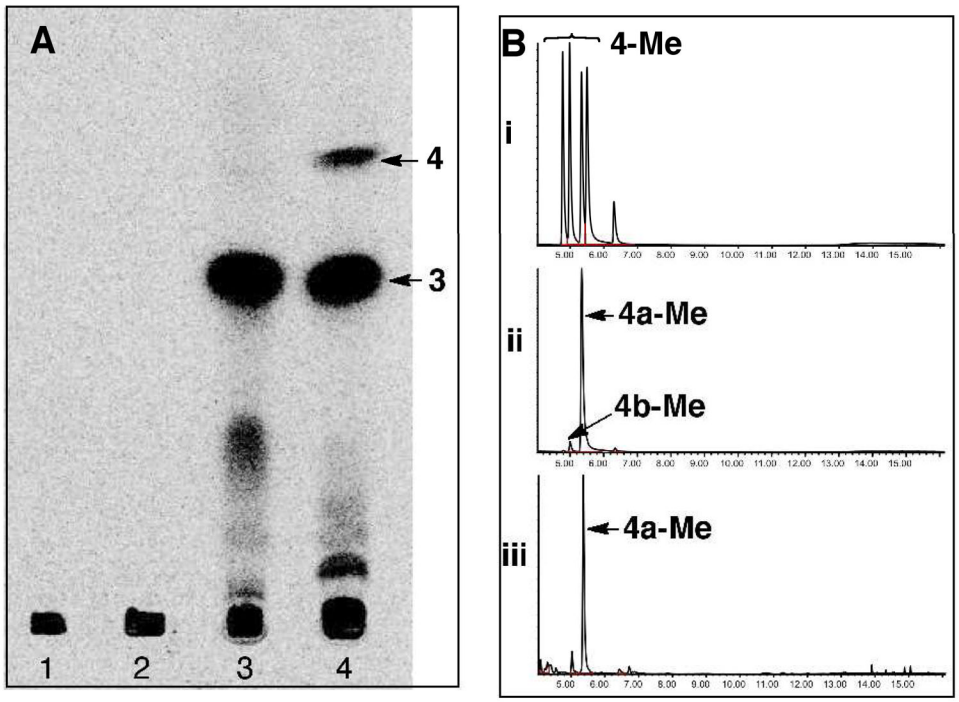

Figure 4.

Incubation of NANS module 2+TE with **2-ACP1** and [2-^{14}C]methylmalonyl-CoA. A. TLC-phosphorimaging, Lanes: 1, without NANS module 2+TE; 2, without **2-ACP1**; 3, without NADPH; 4, with NADPH. B. Chiral GC-EI(+)-MS, SIM mode, *m/z* 88. i. Synthetic mixture of 4 diastereomers of **4-Me**, ret. time 4.78, 4.99, 5.34, and 5.51 min; ii. Synthetic **4b-Me** (ret. time 5.00 min) and **4a-Me** (ret. time 5.35 min); iii. Enzymatically-generated **4a-Me** (ret. time 5.37 min). See Supplementary Figure S3C for mass spectra of synthetic and enzymegenerated **4a-Me**.